Computational Study on the Interactions of Newtonian and Non-Newtonian Fluids in Two-Phase Flow

MS Thesis

by

Maria Kibtiya

CIIT/SP23-RMT-016/LHR

COMSATS University Islamabad

Pakistan

Fall 2024

Computational Study on the Interactions of Newtonian and Non-Newtonian Fluids in Two-Phase Flow

A thesis submitted to

COMSATS University Islamabad

In partial fulfillment

of the requirements for the degree of

Master of Science

in

Mathematics

by

Maria Kibtiya

CIIT/SP23-RMT-016/LHR

Department of Mathematics

Faculty of Science

COMSATS University Islamabad
Pakistan

Fall 2024

Computational Study on the Interactions of Newtonian and Non-Newtonian Fluids in Two-Phase Flow

This thesis is submitted to the Department of Mathematics in partial fulfillment of the requirements for the award of degree of Master in Mathematics.

Name	Registration Number
Maria Kibtiya	CIIT/SP23-RMT-016/LHR

Supervisory Committee

Supervisor

Dr. Muhammad Younas
Associate Professor
Department of Mathematics
COMSATS University Islamabad (CUI)
Lahore Campus

Certificate of Approval

This thesis titled

Computational Study on the Interactions of Newtonian and Non-Newtonian Fluids in Two-Phase Flow

By

Maria Kibtiya

CIIT/SP23-RMT-016/LHR

has been approved

for the Degree of Master in Mathematics

at COMSATS University Islamabad, Lahore Campus

External Examiner: Dr. Khurram Javaid
Northern University (NU) Nowshera, KPK

Supervisor: Dr. Muhammad Younas
Department of Mathematics
CUI, Lahore Campus

Head of Department: Prof. Dr. Muhammad Hussain
Department of Mathematics
CUI, Lahore Campus

Author's Declaration

I Maria Kibtiya, CIIT/SP23-RMT-016/LHR, hereby declare that I have produced the work presented in this thesis, during the scheduled period of study. I also declare that I have not taken any material from any source except referred to wherever due to that amount of plagiarism is within an acceptable range. If a violation of HEC rule on research has occurred in this thesis, I shall be liable to punishable action under the plagiarism rules of HEC.

Date: ____________

____

Maria Kibtiya

CIIT/SP23-RMT-016/LHR

Certificate

It is certified that Maria Kibtiya, CIIT/SP23-RMT-016/LHR has carried out all the work related to this thesis under my supervision at the Department of Mathematics, COMSATS University Islamabad, Lahore Campus and the work fulfills the requirements for award of the degree of MS in Mathematics.

Date: ________________

Supervisor:

____

Dr. Muhammad Younas
Associate Professor
Department of Mathematics
COMSATS University Islamabad
Lahore Campus

Dedication

This thesis is dedicated to my parents, especially my father, for his unwavering support and prayers. I am deeply grateful to my co-supervisor Dr. Mohsan Hassan for their exceptional guidance and to my supervisor Dr. Muhammad Younas for their support. I also dedicate this work to my loved ones for their encouragement and belief in me, and to myself for my dedication to this journey.

Acknowledgements

I begin by expressing my deepest gratitude to ALLAH Almighty (SWT), the Most Gracious, the Most Merciful, for His infinite blessings, strength, and guidance that made it possible for me to complete this thesis. I seek His mercy in all my endeavors. May His peace and blessings be upon the Holy Prophet Muhammad (PBUH), whose life serves as an eternal guide and light in the complexities of this world.

My sincerest thanks go to my supervisor, Dr. Muhammad Younas, for his invaluable support, expert guidance, and consistent encouragement throughout the research process. I am especially grateful to my teacher, Dr. Mohsan Hassan, whose advice and constructive feedback have been crucial in advancing the quality of this work. His insights have been fundamental to the development of this thesis.

I owe a great debt of gratitude to my family, especially my father, for their unwavering support and love throughout my academic journey. Your faith in me has been a constant source of strength, and your sacrifices have made this achievement possible. To my family and friends, your encouragement has been my backbone, and I am eternally grateful.

I would also like to express my appreciation to the Punjab Educational Endowment Fund (PEEF) for their generous scholarship, which provided significant financial support and enabled me to dedicate myself fully to my research.

A heartfelt thank you to my beloved for his continuous support, patience, and understanding throughout this period of my academic life. Your presence has been a great source of comfort and motivation.

I am deeply thankful to everyone who has contributed to this journey. Your encouragement and support have been essential to the successful completion of this thesis.

Maria Kibtiya

CIIT/SP23-RMT-016/LHR

Abstract

Computational Study on the Interactions of Newtonian and Non-Newtonian Fluids in Two-Phase Flow

By

Maria Kibtiya

Two-phase flow implies to the simultaneous movement of two separate phases, such as gases-liquids, liquids-solids, or gases-solids depending on their applications in energy, oil and gas, and chemical processing. This includes slug, bubbling, churn, and mist flows, among others. These flows are modeled using techniques such as the Phase Field Approach, Finite Volume Method, and Euler-Euler model utilizing computational fluid dynamics (CFD) software, COMSOL Multiphysics. This study attempts to examine the laminar two-phase flow of Newtonian (water) and non-Newtonian fluids (polymer using the Carreau model) in a cylinder. Specifically, the goal is to understand the velocity distribution, pressure profiles, and volume fraction distribution and the complicated relationships that exist between Newtonian and non-Newtonian fluids in constrained geometries, relationships that are essential for the optimization of a variety of industrial processes.

Table of Contents

List of Figures

Nomenclature

Variable	Unit	Physical Meaning
$\rho_i, i=1,2$	$\left(kg/m^3\right)$	Fluid density, ρ_1 is the density of Fluid 1 and ρ_2 is the density of Fluid 2
$\boldsymbol{u}$	$\left(m/s\right)$	Velocity vector of the fluid, representing average velocity of both fluids
∇	$\left(m^{-1}\right)$	Del operator, representing spatial derivatives
I		Identity tensor, represents isotropy or the neutral element in tensor operations
$\boldsymbol{\kappa}$	$\left(\mathrm{P}a\right)$	Viscous stress tensor, describes how internal forces are distributed within the fluid
F	$\left(\mathrm{N}/m^3\right)$	A body force term representing interfacial forces and other external forces acting on the fluid
$\boldsymbol{g}$	$\left(m/s^2\right)$	Acceleration due to gravity, corresponding term is $\rho\boldsymbol{g}$
ϕ	$\left(W/m\right)$	Viscous dissipation
$\mu_i, i=1,2$	$\left(\mathrm{P}a\cdot s\right)$	Dynamic viscosity, μ_1 is the dynamic viscosity of Fluid 1 μ_2 is the dynamic viscosity of Fluid 2
μ_{inf}	$\left(\mathrm{P}a\cdot s\right)$	infinite shear viscosity
μ_0	$\left(\mathrm{P}a\cdot s\right)$	Zero-shear viscosity
λ	$\left(s\right)$	Relaxation time
$\dot{\gamma}$	$\left(s^{-1}\right)$	Shear rate
$\boldsymbol{S}$	$\left(s^{-1}\right)$	Strain tensor
n	No units	Flow Behavior Index
$\nabla\boldsymbol{u}$	$\left(s^{-1}\right)$	Velocity gradient tensor
C_p	$\left(J/kg\cdot\mathrm{K}\right)$	Specific heat capacity
$\boldsymbol{q}$	$\left(W/m^2\right)$	Heat Flux

k	$\left(W/_{m\cdot\mathrm{K}} \right)$	Thermal conductivity
$\boldsymbol{Q}$	$\left(W/_{m^3} \right)$	Heat source
$\boldsymbol{Q}_P$	$\left(W/_{m^3} \right)$	Phase Change Heat Source (Latent Heat
$\boldsymbol{Q}_{vd}$	$\left(W/_{m^3} \right)$	Viscous Dissipation Heat Source
T	(K)	Temperature field
$\frac{\partial\phi}{\partial t}$	$\left(s^{-1} \right)$	Time rate of change of the phase field ϕ (order parameter
γ	(no units)	Adjusts the model's relative influence of surface tension and phase separation forces.
λ	(s)	Relaxation time in Carreau Model,
ε	(m)	Interface Thickness Parameter,
ψ	$\left(J/_{m^3} \right)$	Chemical Potential, A thermodynamic potential that controls the evolution of the phase field
F_{st}	$\left(kg/_{m^{2}\cdot s^2} \right)$	The force of surface

Chapter 1

1.1 Fluid

Any material that flows consistently or changes when stressed by shear is applied, regardless of how little force is supplied is referred to as a fluid [1].

Figure 1.1: Fluid

Both liquids and gases are classified as fluids because they do not have a set shape or solid structure and can change to fit the geometry of their containers

1.2 Types of Fluids

Based on their behavior in different scenarios, especially in response to shear stress, fluids can be categorized in several types. The most common types of fluids are as follows [2].

1.2.1 Ideal Fluid

The fluids in question are fictional, incompressible, and lack viscosity or internal resistance. Real fluids always have some degree of viscosity, so these ideal fluids are used in theoretical studies.

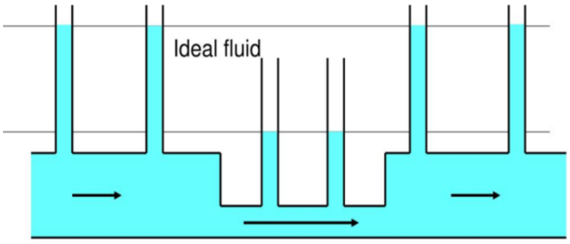

Figure 1.2: Flow of ideal fluid

1.2.2 Real Fluid

These are fluids that are compressible and have a high viscosity. This includes all substances that are actually fluid, such as water, oil, and air.

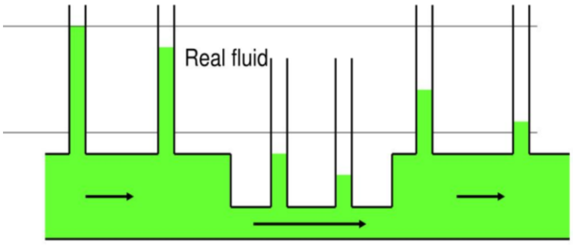

Figure 1.3: Flow of Real Fluid

1.2.3 Compressible Fluid

Compressible fluids like gases experience significant changes in density when pressure changes.

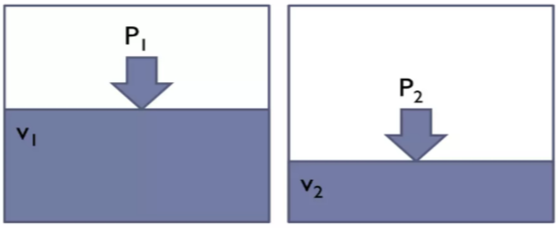

Figure 1.4: Compressible fluid

1.2.4 Incompressible Fluid

Incompressible fluids are defined as having a density that is almost constant regardless variations in pressure. The belief in the incompressibility of liquids is common in many real-world situations.

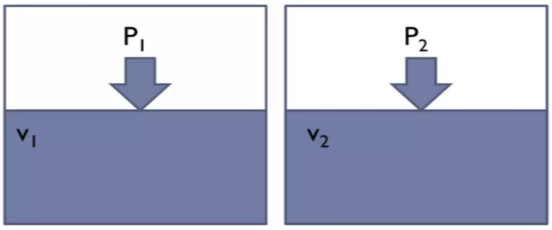

Figure 1.5: Incompressible fluid

1.2.5 Viscous liquid

Significant internal friction (viscosity) is present in these fluids. Honey and other high-viscosity liquids are more resistant to flow than water and other low-viscosity liquids.

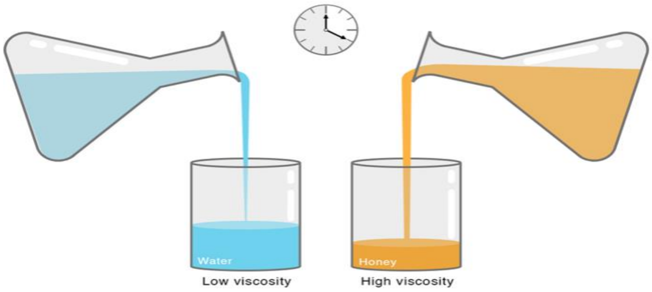

Figure 1.6: Low viscosity and High viscosity Fluid

1.2.6 Ideal Plastic Fluid

These fluids exhibit solid like properties until a specific stress point is applied. They flow like a viscous fluid after reaching the yield pressure.

1.2.7 The Newtonian fluid

Newton's Law of viscosity, states that shear stress is directly proportional to the rate of shear strain (velocity gradient), in fluids that follow this law.

Air, gasoline, and water are just a few examples.

Figure 1.7: Examples of Newtonian Fluids

1.2.8 Non-Newtonian Fluid

The shear stress and shear strain in these fluids exhibit a non-linear relationship. Polymer solutions, ketchup, and blood are a few examples.

Figure 1.8: Examples of Non-Newtonian Fluids

1.3 Types of Non-Newtonian Fluid

Materials that do not adhere to Newton's law of viscosity are known as non-Newtonian fluids. This means that the viscosity is not constant and may change over time, under stress, or with temperature. The primary types include:

1.3.1 Shear-Thinning Fluids (Pseudoplastic)

With an increase in shear rate (faster movement), viscosity decreases. For example, ketchup is easier to pour when squeezed or shaken [3].

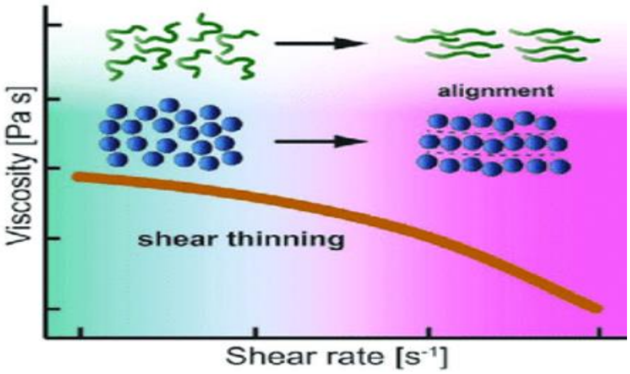

Figure 1.9: Representation of shear-thinning fluids

1.3.2 Shear-Thickening Fluids (Dilatant)

In these fluids, viscosity increases as the shear rate increases. For instance, oobleck, made from cornstarch and water, solidifies when punched [3].

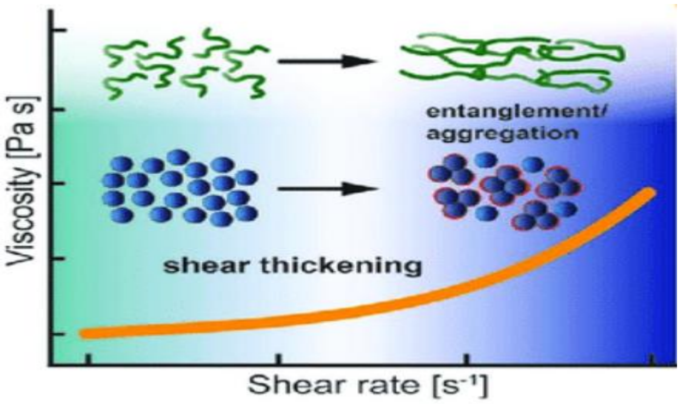

Figure 1.10: Representation of shear- thickening fluids

1.3.3 Bingham Plastics

A minimum stress, or yield stress, is required in order for a substance to begin flowing and exhibit solid-like properties below that threshold [4].

Example: toothpaste

1.3.4 Thixotropic Fluids

Under continuous shear stress, viscosity gradually decreases but can return to its original state [6]. Example: After stirring, the paint flows more easily.

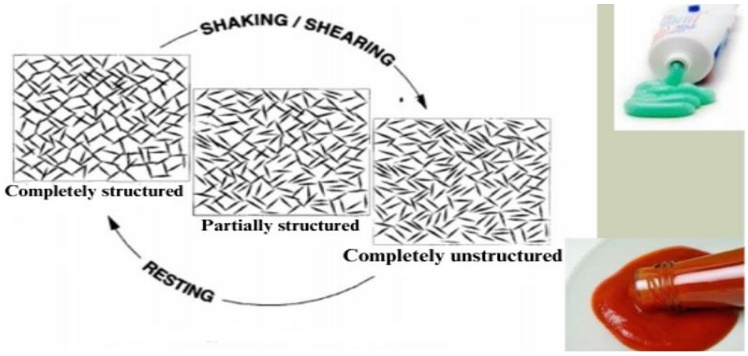

Figure 1.11: Representation of thixotropic fluids

1.4 Flow

A fluid is considered to be in flow when its particles are constantly moving in relation to one another, influenced by an external factor; such as gravity or pressure [1].

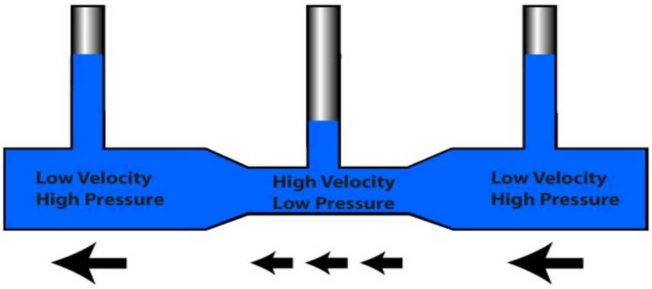

Fig 1.12 Representation of fluid flow

1.5 Types of Flow

In the field of fluid mechanics, flow is categorized according to a number of factors, including system shape, velocity, and viscosity. The primary types of flow are as follows, with descriptions:

1.5.1 Laminar Flow

Laminar flow is defined as fluid flowing in parallel, smooth layers that do not disturb one another. There is minimal mixing between fluid layers, and the flow is orderly Laminar flow is characterized by a Reynolds number (Re) of less than 2,000 [1].

Example: A small-diameter pipe carrying honey or oil.

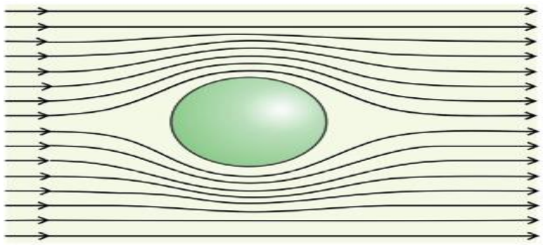

Figure 1.13: Representation of Laminar flow

1.5.2 Turbulent Flow

Turbulent flow is characterized by rapid changes and fluid particle mixing, making it chaotic. The flow contains vortices and eddies, and the velocity fluctuates randomly over time at any given position. Typically, turbulent flow has a Reynolds number (Re) higher than 4,000 [7]. For example, water rushing through a large pipe or air flowing over an airplane wing.

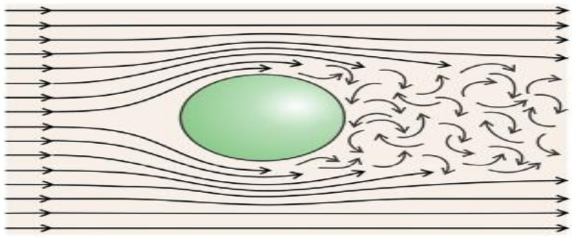

Figure 1.14: Representation of Turbulent flow

1.5.3 Transitional Flow

The zone where a flow displays traits of both laminar and turbulent flow is known as transitional flow. The usual range for the Reynolds number in transitional flow is between 2,000 and 4,000 [2].

An example of this is the flow in pipes as the velocity is continuously raised from low (laminar) to high (chaotic).

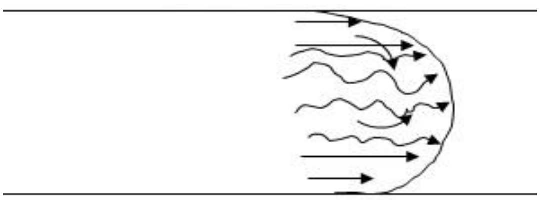

Figure 1.15: Transitional flow

1.5.4 Steady Flow

Steady flow occurs when the characteristics of fluid, such as density, pressure, and velocity, remain constant over time at any given point in the system [8].

For example, water constantly flowing at a constant pressure through a conduit.

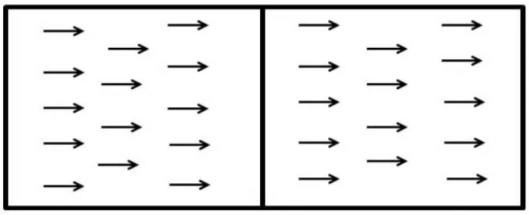

Figure 1.16: Representation of steady flow

1.5.5 Unsteady Flow

The fluid characteristics change over time at any given place in unsteady flow. Unsteady flow is often the result of transient circumstances, such as when a pump is starting or stopping [1]. For example, water flow in a pipe where the valve position abruptly changes.

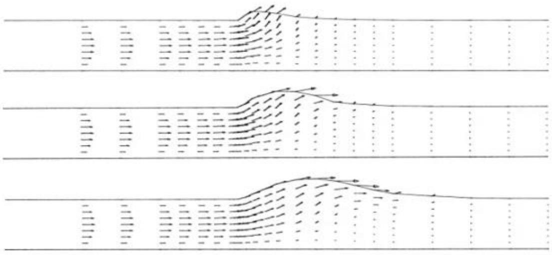

Figure 1.17: Representation of un-steady flow

1.5.6 Compressible Flow

Compressible flow occurs in high-speed gases when pressure changes result in a significant change in fluid density. This typically occurs in gases at high velocities, such as in supersonic or hypersonic flow [9]. For example, when examining the airflow around a fast moving jet.

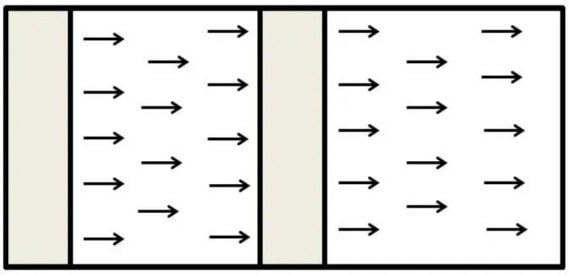

Figure 1.18: Compressible flow

1.5.7 Incompressible Flow

When a fluid flows in an incompressible manner, its density does not change over time. This simplifies the mathematical treatment of fluid dynamics [7].
Example: Water flowing at low velocities through pipes or rivers.

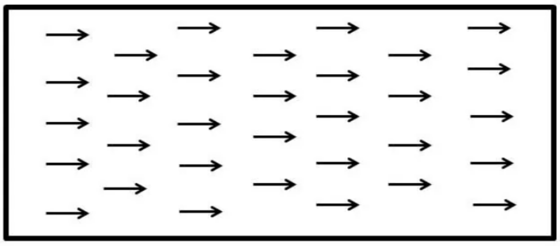

Figure 1.19: Incompressible Flow

1.5.8 Viscous Flow

In viscous flow, the internal friction (viscosity) of the fluid is considered. This friction prevents different fluid layers from moving in relation to each other. Higher viscosity fluids like oil experience greater flow resistance compared to low-viscosity fluids such as water [10]. Example: Molasses flowing through a tube.

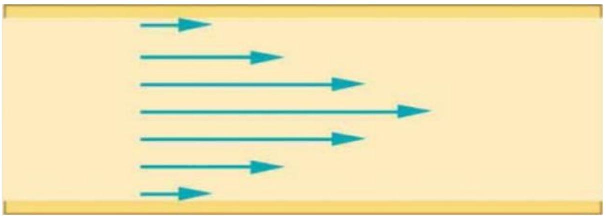

Figure 1.20: Representation of Viscous Flow

1.5.9 Non-viscous Flow

The ideal assumption in fluid mechanics is that the fluid is incompressible and has no.

viscosity. This theoretical concept can simplify the challenges in fluid mechanics. It is important to note that real fluids always have some level of viscosity [16].
For instance: a theoretical study of invisible flow in aero dynamics.

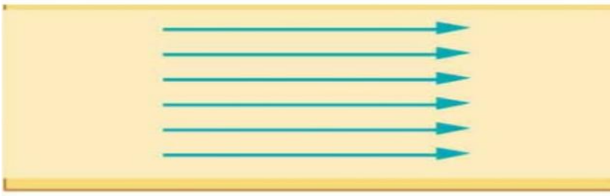

Figure 1.21: Representation of non-viscous flow

1.5.10 Rotational Flow

Fluid particles moving through a fluid in rotational flow exhibit angular motion, or rotation [17].

Example, water in swirling pools or cyclones are two instances of rotational flow.

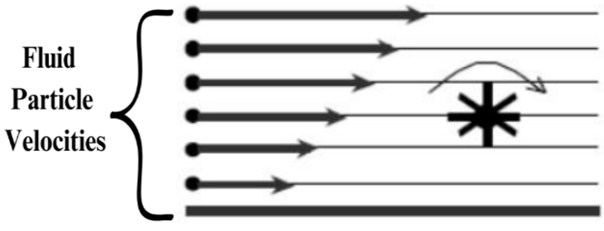

Figure 1.22: Rotational flow

1.5.11 Irrotational Flow

Irrotational flow occurs when fluid particles travel through the fluid without rotating around their own axis [7]. Example: ideal airflow around an airplane wing.

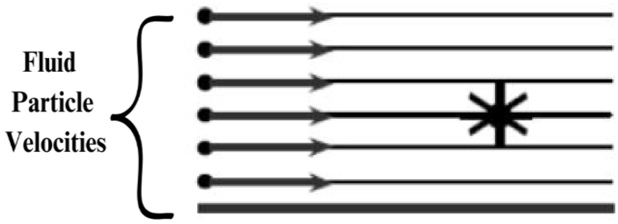

Figure 1.23: Irrotational flow

1.5.12 Single-Phase Flow

When a fluid moves in a single phase that is, as a liquid, gas, or solid without changing phases while doing so, it is referred to as single-phase flow. In single-phase flow, parameters like density, viscosity, and pressure are evenly distributed, and all fluid components act consistently [7]. Example, consider air passing through a ventilation system or water passing through a pipe.

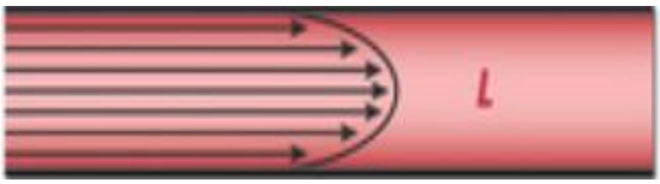

Figure 1.24: Single-phase flow

1.5.13 Multiphase Flow

When two or more phases, such as liquid-liquid, liquid-gas, gas-solid, or liquid-solid with different physical characteristics, such as density or viscosity interact simultaneously within a single system, this is referred to as multiphase flow [11].

For example, in a boiler system, water and steam flow together, or gas and oil flow together in a pipeline.

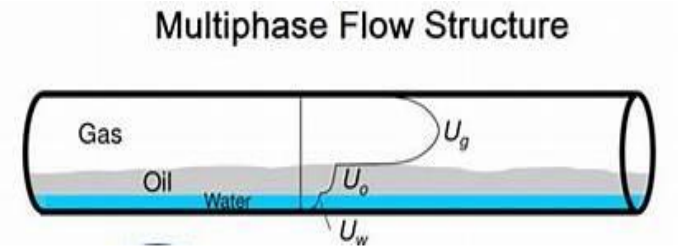

Figure 1.25: Multiphase flow

1.6 Types of Multiphase Flow

The types of flows in multiphase flow are often categorized based on the interaction of different phases, flow pattern, and flow systems. Common multiphase flow patterns, particularly for gas-liquid flows, include [12]

1.6.1 Bubble Flow

It is defined as a continuous phase of liquid with gas bubbles scattered throughout. The bubbles are small and typically dispersed uniformly.

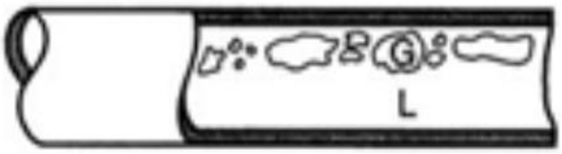

Figure 1.26: Bubble flow

1.6.2 Slug Flow

It is the result of large gas bubbles forming and traveling through the liquid phase, creating sporadic "slugs." Liquid areas and large gas bubbles alternate in the flow.

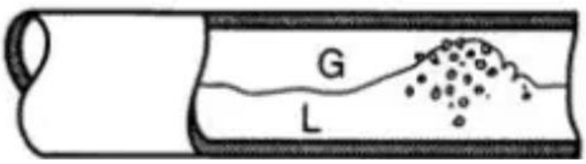

Figure 1.27: Slug flow

1.6.3 Churn Flow

The flow condition is unorganized and extremely chaotic with uneven mixing of liquid and gas bubbles. This flow pattern is typically unstable.

Figure 1.28: Churn flow

1.6.4 Annular Flow

In this setup, a gas core flows through the center, with a liquid film lining the channel walls. The configuration is common in the oil and gas sector for vertical pipelines.

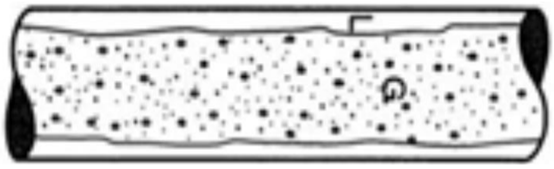

Figure 1.29: Annular flow

1.6.5 Stratified Flow

This phenomenon occurs when liquid and gas flow in separate layers typically through parallel pipes, with the gas flowing at the top and the liquid at the bottom.

Figure 1.30: Stratified flow

1.7 Mathematical models for Two-Phase Flow

The complexity and type of interactions between different phases (such as gas-liquid or liquid-solid) determine the mathematical models used in Computational Fluid Dynamics (CFD) to represent multiphase flows. Each model addresses the issue in its own way, finding a balance between physical accuracy and computational efficiency. The most commonly used mathematical models for multiphase flows in CFD are summarized here.

1.7.1 Euler-Euler Model

Mass balance

For both the continuous and dispersed phases, the following continuity relations apply.

$$\frac{\partial}{\partial t}\left(\rho_c \phi_c\right) + \nabla \cdot \left(\rho_c \phi_c \boldsymbol{u}_c\right) = m_{dc} \tag{1.1}$$

Momentum equation

Using the non-conservative forms, the equations for both continuous and dispersed phases are as follows:

$$\rho_c \phi_c \left[\frac{\partial}{\partial t}\left(\mathbf{u}_c\right) + \boldsymbol{u}_c \nabla \cdot \left(\boldsymbol{u}_c\right)\right] = -\phi_c \nabla \mathrm{P} + \phi_c \nabla \cdot \tau_c + \phi_c \rho_c \boldsymbol{g} + F_{m,c} + \phi_c F_{\mathrm{c}} + m_{dc}\left(\boldsymbol{u}_{\mathrm{int}} - \boldsymbol{u}_c\right) \tag{1.2}$$

1.7.2 The Mixture Model Equations

The phases are treated as a single fluid mixture with a relative velocity between them in the mixture model, making computations easier.

Equations

Mass Conservation for Mixture [13]

$$\frac{\partial \rho_m}{\partial \mathrm{t}} + \nabla \cdot \left(\rho_m \boldsymbol{u}_m\right) = 0$$
$$\text{with } \rho_m = \sum_i \alpha_i \rho_i \tag{1.3}$$

Momentum Conservation for Mixture [14]

$$\frac{\partial\left(\rho_m \boldsymbol{u}_m\right)}{\partial t} + \nabla \cdot \left(\rho_m \boldsymbol{u}_m \boldsymbol{u}_m\right) = -\nabla \mathrm{P} + \rho_m \boldsymbol{g} + \nabla \cdot \mathrm{T}_m + \sum_i \alpha_i \rho_i \boldsymbol{u}_{rel,i} \tag{1.4}$$

1.7.3 Volume of Fluid (VOF) Model

This model is ideal for modeling flows of immiscible fluids with a clear interface, such gas-liquid interfaces [15].

Continuity (Volume Fraction)

$$\frac{\partial \alpha}{\partial t} + \boldsymbol{u} \cdot \nabla \alpha = 0 \tag{1.5}$$

Navier-Stokes with Surface Tension

$$\rho\left(\frac{\partial \boldsymbol{u}}{\partial t} + \boldsymbol{u} \cdot \nabla \boldsymbol{u}\right) = -\nabla \mathrm{P} + \mu \nabla^2 \boldsymbol{u} + \sigma \kappa \delta_s \mathbf{n} \tag{1.6}$$

1.7.4 Level Set Model

The Level Set technique uses a signed distance function to represent the interface between two phases [26].

Level Set Function Evolution

$$\frac{\partial \phi}{\partial t} + \boldsymbol{u} \cdot \nabla \phi = 0 \tag{1.7}$$

Reinitialization Equation

This equation ensures ϕ remains a signed distance function:

$$\frac{\partial \phi}{\partial \tau} = sign(\phi_0)(1 - |\nabla \phi|) \tag{1.8}$$

1.7.5 Phase Field Model

The Phase Field model demonstrates the occurrence of each phase on a diffuse surface, through a smooth transition between phases, using a continuous variable (order parameter) [17].

Cahn-Hilliard Equation (governing the phase field variable):

$$\frac{\partial \phi}{\partial t} + \boldsymbol{u} \cdot \nabla \phi = \nabla \bullet (\mathrm{M} \nabla \mu) \tag{1.9}$$

where,

$$\mu = \frac{\delta F}{\delta \phi}$$

Navier-Stokes Equations with Phase Field Coupling

$$\rho\left(\frac{\partial u}{\partial t} + \boldsymbol{u} \cdot \nabla \boldsymbol{u}\right) = -\nabla \mathrm{P} + \nabla \cdot \left(\mu\left(\nabla \boldsymbol{u} + (\nabla \boldsymbol{u})^{\mathrm{T}}\right)\right) + \boldsymbol{F}_{\mathrm{int}erface} \tag{1.10}$$

Chapter 2

2.1 Introduction

Two-phase flow is commonly used in the chemical, oil, gas, and energy sectors. It involves the movement of two different phases, such as gas-liquid or liquid-solid. In order to simulate two-phase flows, CFD programs like COMSOL Multi-physics utilize Euler-Euler or Euler-Lagrange methods as well as models like the Phase Field Approach. While these methods are effective in capturing phase interactions, achieving accurate results requires careful consideration of accuracy and computing costs.

2.2 Literature Review

Various characteristics associated with two-phase flows have been the focus to multiple researches. Seungjin et al. [18] estimate the concentration of interfacial area that varies from bubble to churn-turbulent flow by utilizing the dynamic Interfacial Area Transport Equation (IATE) in circular, spherical and rod-bundle designs. Guanxi et al. [19] applied the Level-Set Model (LS) to porous materials to investigate various theories for modeling dynamic non-equilibrium processes and their scientific uses in geotechnics. Ayodeji et al. [20] studied two-phase flow in a 5 x 5 square rod bundle using the Euler-Euler model. The study demonstrated how partial blockage impacts two-phase flow behavior in a 5 x 5 rod bundle, showing notable modifications in velocity distribution and pressure reduction down streams of the obstruction. Darioush et al. [21] used the Level Set method in channels and pipes to demonstrate the clarity and stability of Physics Informed Neutral Networks (PINNs) in modeling multiphase flows with heat transfer, emphasizing their potential for a variety of useful applications. Guangming et al. [22] studied two-phase flow using an Euler–Bernoulli beam model in a functionally graded pipe conveying gas-liquid two-phase flow. The results revealed that stability is improved by a higher elastic modulus gradient, while stability is compromised by high density gradient and boundary constraints. Alexandra et al. [23] examined non-equilibrium effects of a decrease in pressure in a CO_2 pipe by applying a homogeneous equilibrium model (HEM). The results showed that at high temperatures, equilibrium increased, while at lower temperatures, there was prolonged vapor creation along with pressure obstructions. Yixiang et al. [24]

used the ISPH-FVM (incompressible smoother particle hydrodynamics-Finite volume method) coupling method to investigate whether the CSF (continuum surface force) and CSS (continuous surface stress) models are better at effectively capturing complex variations in the ISPH-FVM model compared to the HF (height function). Abdullah et al. [25] investigated two-phase flow in a tube fitted with a concave sensor using a CFD approach. The results showed that the MLP neural network does not require adjustments as it estimates vacuum fractions with a Mean Absolute Error (MAE) of 1.74, regardless of variations in liquid phase density. Younes et al. [26] utilized 3D CFD simulation in a serpentine micro-channel to examine flow patterns. They demonstrated the transition from slug flow to parallel flow of plugs as the flow rate increased. Rundi et al. [27] investigated two-phase flow in 2D domain using the phase-field method. The study demonstrates the accuracy of PF-PINNs. PF-PINNs effectively handle high-order variations without sacrificing efficiency, and they demonstrate excellent consistency with the reference information. Ali Ebrahimi-Mamaghani et al. [28] conducted a study on two-phase flow using the Drift-Flux model to analyze the vibrations of supported pipes, both linear and nonlinear. The study found that the vibration rate of the system varied significantly between different flow patterns due to two-phase damping caused by flow parameters and pipe shape. Chun et al. [29] investigated two-phase flow using Drift-Flux equations in one-dimensional inclined pipes to examine the exact Riemann solutions of the drift-flux equations under gravity. The study provided a thorough verification of the validity of the solutions and identified occurrences such as curved delta shock waves and vacuum conditions. Suhas S. Jain [30] explored two-phase flow including droplets in a shear flow, using the phase-field method to investigate how the suggested phase-field model preserves the mass of each phase and guarantees finite transport of the volume fraction. It is precise, conservative, bounded, and resilient. Roman W. Morse et al [31] utilized a pore network model (PNM) and real 3D pore structures from micro-CT imaging to study how fluid flow during hydrate extraction is affected by the anisotropic permeability evolution resulting from the shearing of hydrate-bearing sediments (HBS). Zhe Lin et al [32] utilized the CFD-Discrete Element Method model and two-dimensional gate valve geometry to analyze erosion and two-phase flow properties between gas and solid. The simulation offers valuable insights for constructing more erosion-resistant valves, by revealing that particle size and valve opening significantly impact particle dispersion and erosion. The hollow part of the valve experienced more severe erosion compared to the flashboard.

Chapter 3

Computational Study on the Interactions of Newtonian and Non-Newtonian Fluids in Two-Phase Flow

Two-phase flow, which is essential in areas involving energy, oil and gas, and chemical processing, involves the movement of two separate phases, such as gas-liquid or liquid-solid. Laminar two-phase flow of Newtonian and non-Newtonian fluids in a cylinder is simulated using CFD programs like COMSOL Multi-physics utilizing technique like Phase Field. In multiphase flows, material science, heat transfer, and biological systems, the Phase Field Method is a numerical method for simulating interfacial dynamics. It improves energy applications, environmental studies, and industrial processes by modeling intricate interface behaviors without the need for explicit tracking. Our analysis focuses on understanding the presence of both phases, velocity distribution, pressure profiles, and volume fraction distribution within the system. This research seeks to provide insights into the complex interactions between Newtonian and non-Newtonian fluids in confined geometries, which are critical for optimizing various industrial processes.

3.1 Mathematical Model

Governing equations are crucial mathematical equations used to explain physical processes. Two-phase flows require additional equations for mass, momentum, and energy conservation. In fluid dynamics, motion of fluid is modeled by the Navier-Stokes equations. Phase interfaces can be tracked using technique like the volume of fluid (VOF) method. The Phase Field Method is a numerical method for simulating interfacial dynamics. To simulate complicated systems, including multi-phase flows in industrial applications, these equations are frequently solved numerically using techniques like finite volume or finite element approaches.

The main governing equations for two-phase flow and fluid dynamics are as follows:

3.1.1 Continuity equation

$$\rho \nabla \cdot \boldsymbol{u} = 0 \tag{3.1}$$

3.1.2 Momentum equation

The incompressible formulation of the Navier-Stokes equations is automatically applied in Phase Field interfaces.

$$\rho\left(\boldsymbol{u}\cdot\nabla\right)\boldsymbol{u}=\nabla\cdot\left(-\mathrm{P}I+\boldsymbol{\kappa}\right)+F+\rho\boldsymbol{g} \tag{3.2}$$

Where

$$\boldsymbol{\kappa}=\mu\left(\nabla\boldsymbol{u}+\left(\nabla\boldsymbol{u}\right)^{\mathrm{T}}\right),$$

$$\rho=\rho_1\phi+\rho_2\left(1-\phi\right),\mu=\mu_1\phi+\mu_2\left(1-\phi\right)$$

Please note that Equation 3.1, and 3.2 are resolved within the confined interface of Laminar Flow. The behavior of non-Newtonian fluids is often studied using the constitutive equation known as the Carreau model. This model accurately describes the shear-thinning or shear-thickening behavior seen in these materials by linking the fluid's viscosity to the applied shear rate.

Carreau model

The non-Newtonian behavior of shear-thinning fluids is mathematically described by the Carreau model. These fluids become less viscous as the shear rate increases. This model is commonly used in rheology and CFD to simulate the flow of complex fluids, such as biological fluids, polymer solutions, and certain suspensions. The values of material properties for the Carreau model are given in Table 3.2.

For fluid 2

$$\mu_{\mathrm{app}_2}=\mu_{\mathrm{inf}}+\left(\mu_0-\mu_{\mathrm{inf}}\right)\left[1+\left(\lambda\dot{\gamma}\right)^2\right]^{\frac{n-1}{2}} \tag{3.3}$$

3.1.3 Energy Conservation

$$\rho C_{\mathrm{P}}\boldsymbol{u}\cdot\nabla\mathrm{T}+\nabla\cdot\boldsymbol{q}=Q+Q_{\mathrm{P}}+Q_{vd} \tag{3.4}$$

Where $\boldsymbol{q}=-k\nabla\mathrm{T}$

3.1.4 Phase Field Equation (Interface Tracking)

The following equations are used when tracking the interface with the phase field method.

$$\frac{\partial\phi}{\partial t}+\boldsymbol{u}\cdot\nabla\phi=\nabla\cdot\frac{\gamma\lambda}{\varepsilon^2}\nabla\psi \tag{3.5}$$

Where

$$\psi=-\nabla\cdot\varepsilon^2\nabla\phi+\left(\phi^2-1\right)\phi$$

3.1.5 The Surface Tension Force

In the phase field approach, the surface tension force is applied as a body force.

$$F_{st} = \left(\frac{\lambda}{\varepsilon_{pf}^2}\psi - \frac{\partial f}{\partial \phi} \right) \nabla \phi$$

$\dfrac{\partial f}{\partial \phi}$ is an energy source that is user-defined.

3.1.6 The Volume Force and Gravity Force

A force derived from a user-defined source of free energy is determined using a Phase Field interface as detailed below:

$$\boldsymbol{F}_{ext} = \left(\frac{\partial f}{\partial \phi} \right) \nabla \phi$$

When a ϕ-derivative of the external free energy is defined in the external free energy of the Fluid Properties, this force is added.

$\boldsymbol{g}$, the gravity vector.in the gravity force $\rho \boldsymbol{g}$.

3.2 Geometry

We built a larger horizontal cylinder oriented along the x-axis with a radius of 10 cm and a length of 150 cm. This cylinder represents the primary flow zone containing a non-Newtonian fluid, referred to as domain 1. Inside this cylinder, we placed several spherical drops, each with a radius of 2 cm, at various points. These drops are labeled as domains 2, 3, 4, representing Newtonian fluid. The combination of the embedded spheres and the large cylinder forms the entire system, which includes both an outlet and an inlet. The boundaries of the system adhere to non-slip conditions. At the inlet, we set the velocity profile and temperature for the non-Newtonian fluid (Fluid 2), also known as Inflow 1. Water, a Newtonian fluid (Fluid 1), fills the droplets inside the cylinder. This setup aims to observe the flow behavior and temperature distribution within the combined structure to study the interactions between the two fluids.

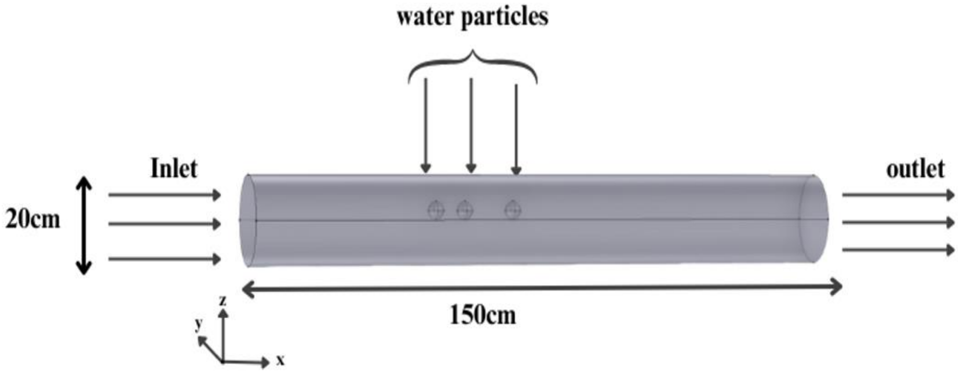

Fig. 3.1: The investigated geometric structure

Table 3.1: Boundary Description Table

Properties	**Inlet**	**Outlet**
Velocity $(\boldsymbol{u})$	$1.2\left(m/s\right)$	
Temperature (T)	453.15K	
Pressure (P)		$0Pa$

3.3 Numerical Simulations

COMSOL Multi-physics is used to model the temperature and velocity distributions of the system. The software simulates the interaction between Newtonian droplets and the non-Newtonian fluid under predetermined intake and boundary parameters.

3.3.1 Meshing

Meshing, which breaks the geometry into smaller components for precise computing, is an essential stage in numerical simulations using COMSOL. Depending on the requirements of the problem, it generates structured or unstructured meshes to ensure the resolution of complex geometries and physical phenomena. Accurate solutions are achieved while maintaining computational efficiency through proper meshing.

The system's mesh can be seen below.

Fig. 3.2 Mesh of the investigated geometric structure

Table 3.2: Summary of mesh elements

Sequence Type	
Physics-controlled-mesh	
Element size	Fine
Geometric Entity Selection	
Geometric entity level	Entire geometry
Element Quality	
Quality measure	Skewness
Statistics	
Complete mesh	
Mesh vertices	343,649
Element type	All elements
Tetrahedra	1,780,546
prisms	75,248
triangles	41,496
quads	336
edge elements	1,092
vertex elements	26
Domain element statistics	
Number of elements	1,855,794
Minimum element quality	0.147
Average element quality	0.6908
Element volume ratio	0.03373
Mesh volume	47,090 cm^3

Table 3.3: Variables used in Carreau model

Name	**Symbol**	**Unit**	**Value**
Viscosity at Zero shear rate	μ_0	$(\mathrm{P}a \cdot s)$	2000
Viscosity at Infinite shear rate	μ_{inf}	$(\mathrm{P}a \cdot s)$	100
Relaxation time	λ	(s)	0.1
Power Index in Case 1	n	No units	0.3
Power Index in Case 2	n	No units	0.4

3.3.2 Convergence Graphs

In COMSOL, convergence or error graphs are used to indicate the accuracy and stability of numerical solutions. These graphs show the decrease in errors or residuals during iterative calculations, they ensuring that the result meets predetermined limitations. In Fig. 3.3 for both $n=0.3(a), n=0.4(b)$, the error significantly decreases in the initial iterations, especially for velocity $\boldsymbol{u}$ and pressure P, as seen in the convergence graphs for the segregated solver. The iterations show slight oscillations as the temperature and phase field variables converge at a slower rate. A higher degree of shear thinning results in faster convergence for $n=0.3$, leading to a more consistent solver performance. With errors stabilizing at very low values for all variables, both scenarios successfully achieve convergence.

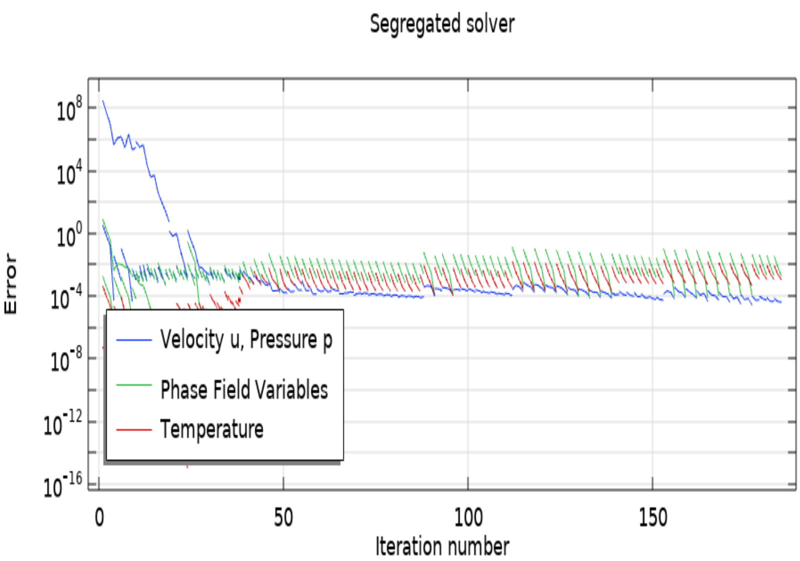

(a)

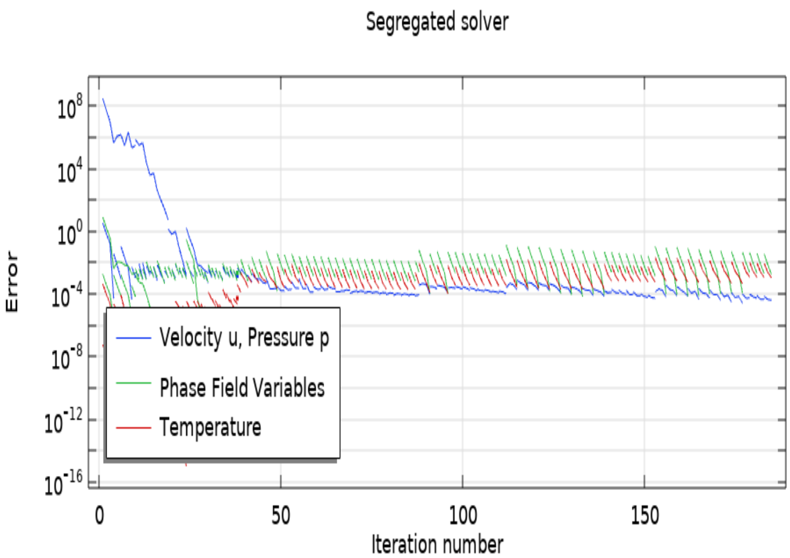

(b)

Fig. 3.3 Convergence Graph for $n = 0.3(a)$ and $n = 0.4(b)$

3.4 Results and Discussions

3.4.1 Velocity and Temperature profiles

In the Figure 3.4 (a) and (b), the velocity $(\boldsymbol{u})$ is plotted against the x-axis across a range of time intervals ($0s$ to $0.5s$) on the graph. The curves illustrate the distribution of velocity for $n = 0.3(a)$ and $n = 0.4(b)$, which initially increases, reaches a peak, and then symmetrically decreases. The changes over time depict how the flow profile is dynamically evolving.

In the Figure 3.5 (a) and (b), the temperature distribution at various time intervals along the x-axis is displayed. For both $n = 0.3(a)$ and $n = 0.4(b)$, the temperature remains constant at $t = 0s$, representing the initial state of the system. At $t = 0.1s$, the imposed boundary condition of 453.15K causes a slight temperature increase the entrance. As time progresses, from ($t = 0.2s$ - $t = 0.5s$), the temperature continues to rise peaking near the center as it spreads further into the domain. The slow increase downstream and the sharp gradient near intake highlight the conduction-dominated transient heat transport.

3.4.2 Velocity and Temperature Contours

The effects of velocity and temperature on fluid flow and droplet behavior at different time intervals are illustrated and described in a cylinder. The analysis demonstrates how changes in temperature and velocity gradients impact droplet stability and dispersion for both $n = 0.3(a)$ and $n = 0.4(b)$.

According to Figure 3.6 (a) and (b), the concentration of water droplets is around $x = 55cm$ at $t = 0s$. This is particularly evident in the center of the domain where the flow dynamics are the sharpest. The droplets scatter as the mainstream fluid begins to move and interact with them, resulting in an increase in velocity due to the initial mixing of the droplets with the mainline flow. The start of fluid mixing and droplet movement occurs at this dispersion point. It is worth noticing that the findings for $n = 0.3(a)$ and $n = 0.4(b)$ are currently the same, suggesting that the power index has no discernible effect on the behavior of the system in the early stages. This dispersion marks the beginning of droplet movement and fluid mixing.

The droplets travel the entire length of the domain in the figure 3.7 (a) and (b) at $t = 0.1s$, reaching about $x = 70cm$. The color legend shows that for both $n = 0.3(a)$ and $n = 0.4(b)$, the red hue in the middle indicates that the droplets are moving quickly in this area, suggesting strong acceleration and significant interaction with the mainstream fluid. The droplets are dispersing, as shown by the transition from red to blue. Their velocity is highest near the center of the flow and gradually decreases as they approach the boundaries. In both cases, this illustrates how the flow and droplet mixing dynamics produce a non-uniform velocity profile.

The Figure 3.8 (a) and (b) at $t = 0.2s$ shows that, the droplets have traveled further and are now at $x = 90cm$. As the droplets move towards the outside edges, their velocity decreases. However, the center, indicated by the red area still maintains the highest velocity, indicated by the color legend. This indicated that the flow is carrying the droplets, causing them to continue spreading out as the move downstream. The influence of the mainline flow is demonstrated by the high velocity near the center, and dispersion becomes more noticeable as the domain lengthens. This behavior remains consistent for both $n = 0.3(a)$ and $n = 0.4(b)$, showing consistent outcomes in both situations.

In the Figure 3.9 (a) and (b), it is clearly seen that at $t = 0.3s$ for $n = 0.3(a)$ and $n = 0.4(b)$, the droplets are visibly moving along the length of cylindrical domain, and as they approach $x = 100cm$, their intensity and velocity increase. It seems that the droplets' velocity initially increase, peaking near the center, and then either stabilizes or decreases as they moved downstream. The dynamic interaction between the droplets and the surrounding fluid is emphasized by the velocity profile and distance traveled, which align with underlying flow conditions, as can clearly be seen in Figure 3.9 (a) and (b).

In the Figure 3.10 (a) and (b), at $t = 0.4s$, the droplets have traveled to $x = 130cm$. Higher velocity is indicated by the red core in the color legend, where the flow speed is faster than at the edges. The mainstream fluid velocity, which falls near the margins, is more in line with the dispersed droplets. Drag forces result in small variations in the velocity of droplets in areas of different velocities. However, the outcomes remain the same in both situations.

Figure 3.11 (a) and (b) explains that, at $t = 0.5s$, the droplets are fully dispersed, having traveled a distance of $x = 150cm$. High velocity (red) represented in the middle of the droplets while lower velocities are shown at the corners. Aligning with the fluids' profile, which is slower at the edges and faster in the middle, the droplets are now following the mainstream fluid. This demonstrates how the flow and mixing dynamics of the droplets produce same behavior in both cases.

The figure 3.12 (a) and (b) displays the temperature distribution at $t = 0.1s$, with cooler tones (Blue) downstream and higher temperatures (Red, $\approx 460K$) close to the intake. This trend is consistent for both $n = 0.3(a)$ and $n = 0.4(b)$, indicating that the thermal distribution is mainly determined by heat transfer and flow near the entrance and is not significantly affected by the power index in the Carreau model.

The figure 3.13 (a) and (b) depicts the temperature distribution at $t = 0.2s$, showing lower temperatures downstream (Blue) transitioning from high temperatures near the inlet (Red, $\approx 460K$). The temperature gradient indicates heat dissipation along the domain, highlighting strong thermal interactions near the entrance. This pattern remains consistent for both $n = 0.3(a)$ and $n = 0.4(b)$, suggesting that the fluid's physical properties play a secondary role in heat transfer and flow dynamics.

The figure 3.14 (a) and (b) depicts the temperature distribution of the cylinder at $t = 0.3s$. Higher temperatures (Red, $\approx 460K$) transition to cooler tones (Blue) downstream, show a clear temperature gradient near the inlet. The consistent profiles for $n = 0.3(a)$ and $n = 0.4(b)$ indicate that the power index has minimal impact on the thermal distribution, emphasizing the significance of heat transport near the inlet.

The figure 3.15 (a) and (b) depicts the temperature distribution of the cylinder at $t = 0.4s$. Higher temperatures (Red $\approx 460K$) transition to cooler tones (Blue) downstream in a clear temperature gradient that is noticeable near the inlet. Heat transport close to the inlet is emphasized by consistent profiles for $n = 0.3(a)$ and $n = 0.4(b)$, showing minimal influence from the power index.

The figure 3.16 (a) and (b) shows, higher temperatures near to the intake suggest strong thermal interaction, with temperatures ranging from $300K$ (Blue) to $460K$ (Red) at $t = 0.5s$. Subsequently, the temperature decrease and stabilizes. This trend, which illustrates the limited impact of the power index on thermal behavior, remains consistent for $n = 0.3(a)$ and $n = 0.4(b)$.

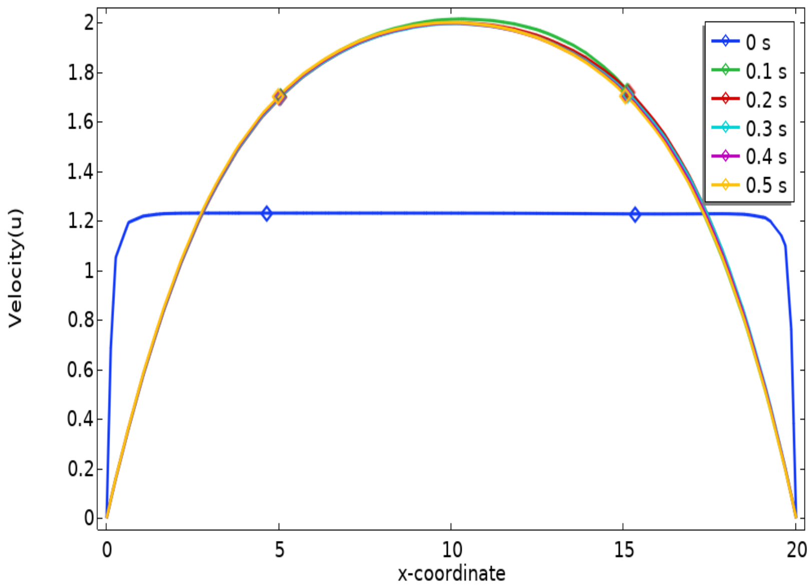

Fig 3.4(a): Velocity$\left(\boldsymbol{u}\right)$ profile at $n = 0.3$.

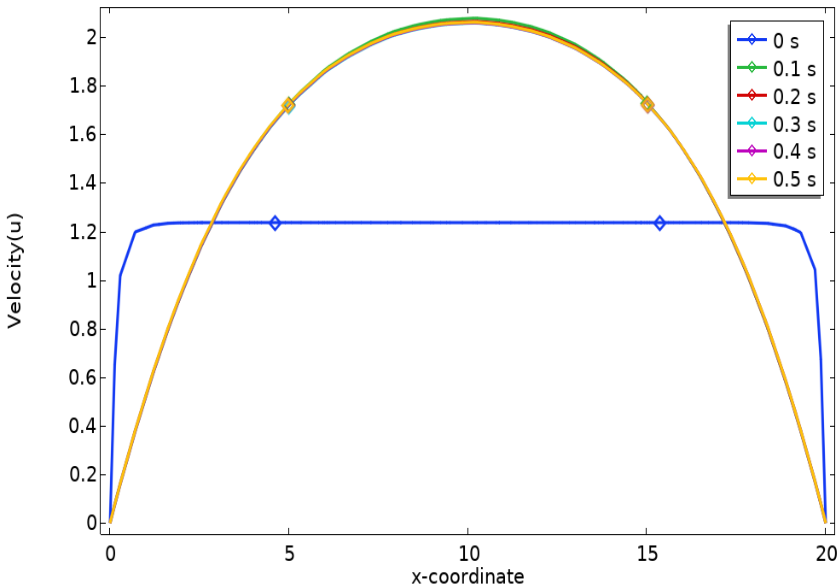

Fig 3.4(b): Velocity$\left(\boldsymbol{u}\right)$ profile at $n = 0.4$

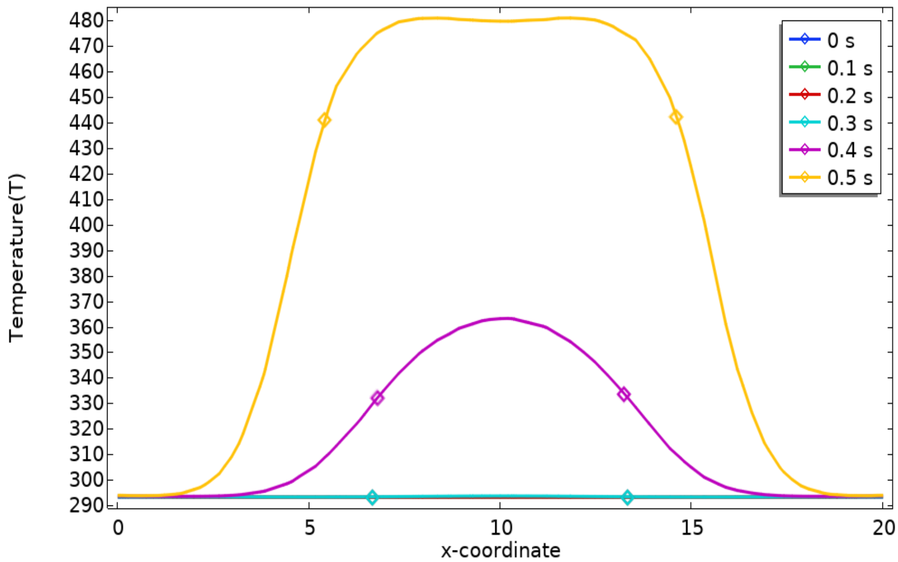

Fig 3.5(a): Temperature (T) profile at $n = 0.3$.

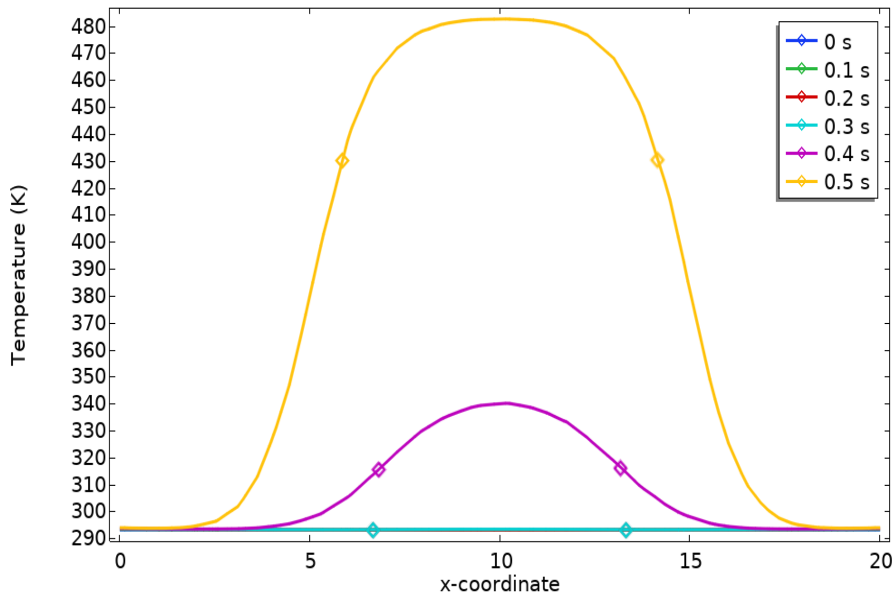

Fig 3.5(b): Temperature (T) profile at $n = 0.4$.

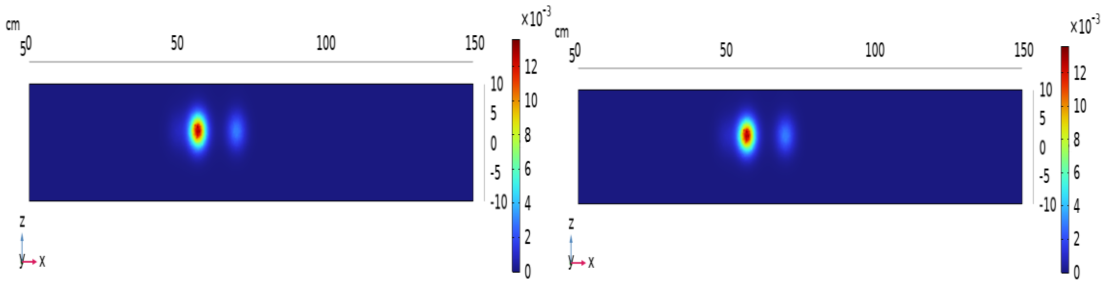

Fig 3.6 Dispersion of water droplet in non-Newtonian fluid for $n = 0.3(a)$, $n = 0.4(b)$ at $t = 0s$

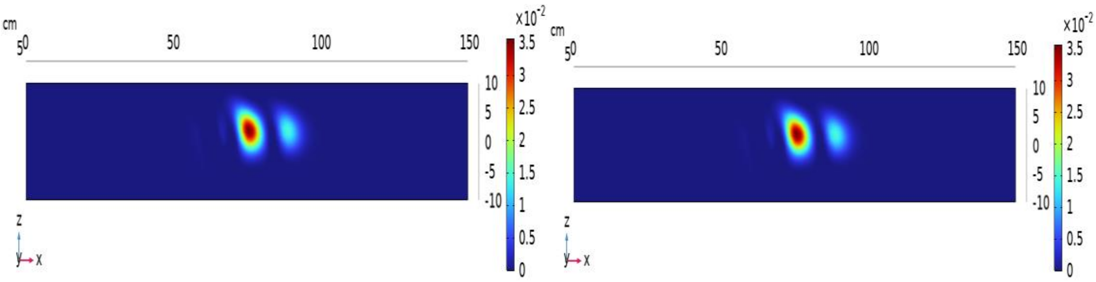

Fig 3.7 Dispersion of water droplet in non-Newtonian fluid for $n = 0.3(a), n = 0.4(b)$

at $t = 0.1s$

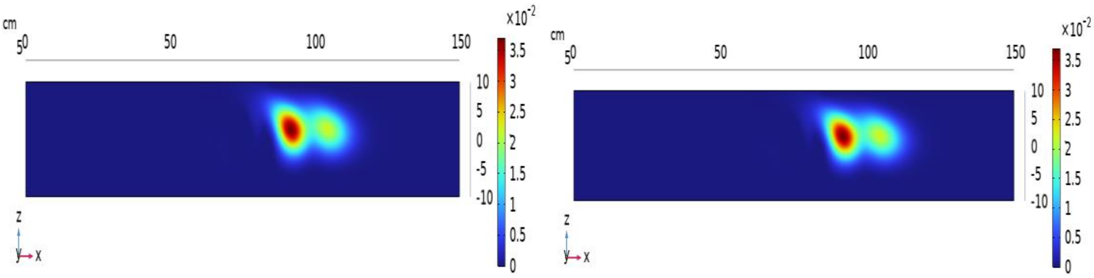

Fig 3.8 Dispersion of water droplet in non-Newtonian fluid for $n = 0.3(a), n = 0.4(b)$

at $t = 0.2s$

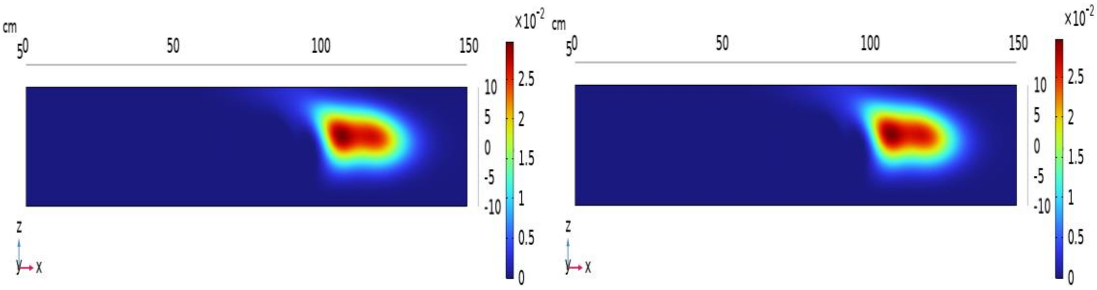

Fig 3.9 Dispersion of water droplet in non-Newtonian fluid for $n = 0.3(a)$, $n = 0.4(b)$

at $t = 0.3s$

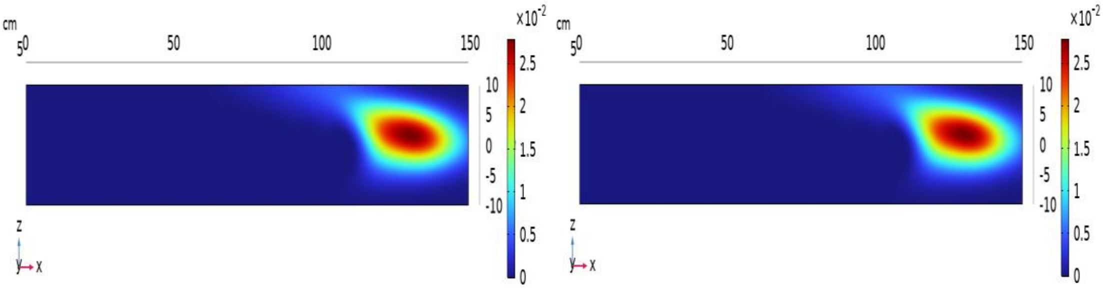

Fig 3.10 Dispersion of water droplet in non-Newtonian fluid for $n = 0.3(a)$, $n = 0.4(b)$

at $t = 0.4s$

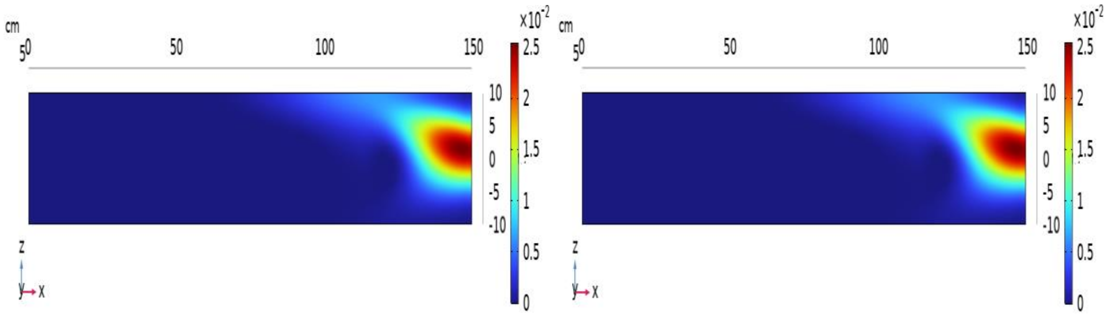

Fig 3.11 Dispersion of water droplet in non-Newtonian fluid for $n=0.3(a)$, $n=0.4(b)$ at $t=0.5s$

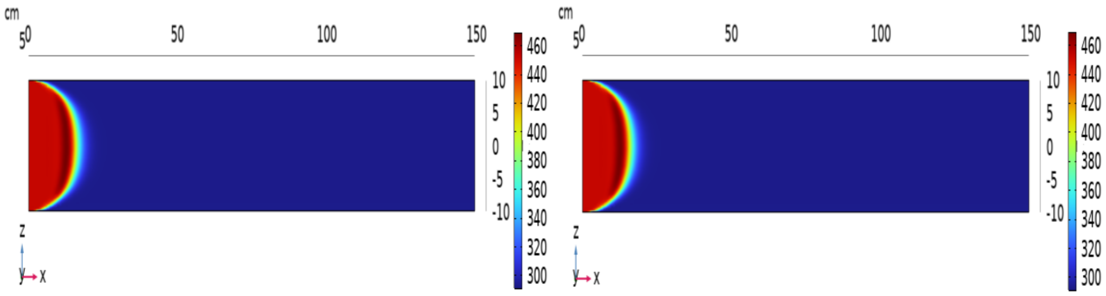

Fig 3.12 Temperature contours for $n=0.3(a)$, $n=0.4(b)$ at $t=0.1s$

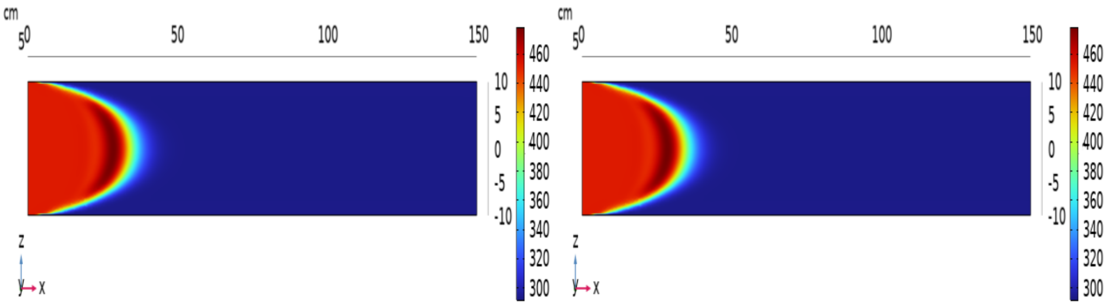

Fig 3.13 Temperature contours for $n=0.3(a)$, $n=0.4(b)$ at $t=0.2s$

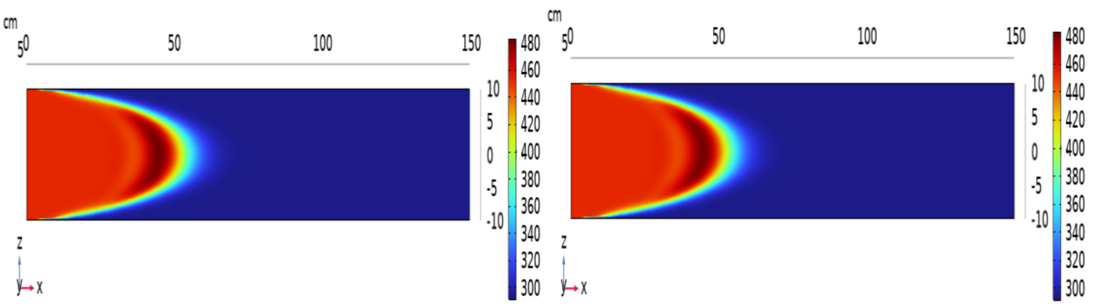

Fig 3.14 Temperature contours for $n=0.3(a)$, $n=0.4(b)$ at $t=0.3s$

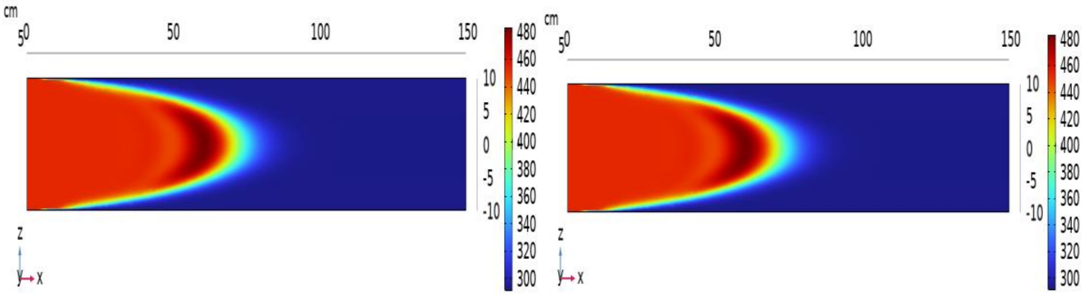

Fig 3.15 Temperature for $n = 0.3(a)$, $n = 0.4(b)$ at $t = 0.4s$

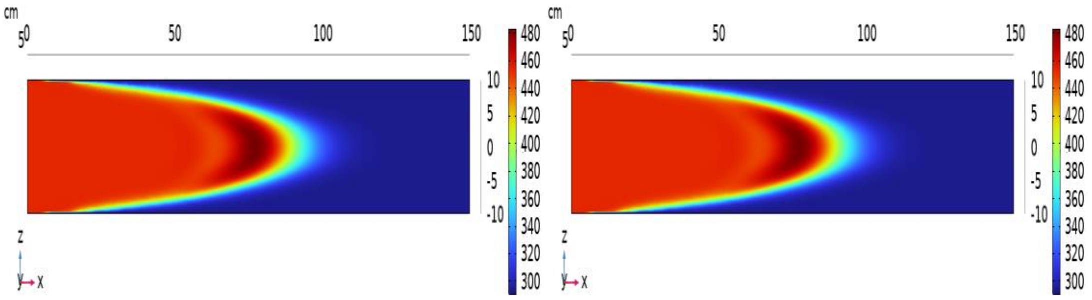

Fig 3.16 Temperature for $n = 0.3(a)$, $n = 0.4(b)$ at $t = 0.5s$

3.5 Conclusion

The study utilizes COMSOL to model a cylindrical structure containing spherical Newtonian drops within a non-Newtonian fluid. The Phase Field approach is employed to analyze fluid interactions using two different power index values. The study produces volume fraction, velocity, and temperature contours, as well as convergence graph for the two power index values.

For Velocity Profiles

- At $n = 0.3$, stronger shear-thinning results in sharper velocity gradients, higher peak velocities, and faster flow production with a distinct parabolic shape.
- At $n = 0.4$, the shear-thinning is weaker, resulting in smoother curves, slower flow development, and lower peak velocities.
- A smaller n increases convection heat exchange by decreasing viscosity, whereas a larger n maintains viscosity and depends more on conduction. Both achieve parabolic profiles, but $n = 0.3(a)$ does faster.

For Temperature Profiles

- At $n = 0.3$, stronger shear-thinning improves convective heat transport, resulting in higher, faster heat generation, and a quicker temperature rise.

- Conversely, at $n = 0.4$, the smaller shear-thinning, leads to slower heat transfer, low temperature peak, and depends more on conduction.
- A greater value of n reduces temperature transmission by providing localized heating close to the input, while a smaller value of n promotes faster, and more even heating.

References

[1] White, F. M. (2016). Fluid Mechanics 8th Ed., 8th Edition

[2] Pritchard, P. J. (2015). *Fox and McDonald's Fluid Mechanics*. Wiley.

[3] Barnes, H. A. (1989). Shear‐thickening ("Dilatancy") in suspensions of nonaggregating solid particles dispersed in Newtonian liquids.*Journal of Rheology*, *33*(2), 329-366.

[4] Bingham, E. C. (1922). *Fluidity and plasticity*. McGraw-Hill.

[6] Mewis, J., & Wagner, N. J. (2009). Thixotropy. *Advances in colloid and interface science*, *147*, 214-227.

[7] Munson, B. R., Rothmayer, A. P., & Okiishi, T. H. (2012). *Fundamentals of fluid mechanics*. Wiley Global Education.

[8] Douglas, J. F. (2005). *Fluid mechanics*. Pearson education.

[9] Shapiro, A. H. (1953). The dynamics and thermodynamics of compressible fluid flow. *New York: Ronald Press*.

[10] White, F. M., & Majdalani, J. (2006). *Viscous fluid flow* (Vol. 3, pp. 433-434). New York: McGraw-Hill.

[11] Wallis, G. B. (2020).*One-dimensional two-phase flow*. Courier Dover Publications.

[12] "Kunii, D., & Levenspiel, O. (2013). *Fluidization engineering*. Elsevier.

[13] Manninen, M., Taivassalo, V., & Kallio, S. (1996). On the mixture model for multiphase flow.

[14] Ishii, M., & Hibiki, T. (2010). *Thermo-fluid dynamics of two-phase flow*. Springer Science & Business Media.

[15] Hirt, C. W., & Nichols, B. D. (1981). Volume of fluid (VOF) method for the dynamics of free boundaries. *Journal of computational physics*, *39*(1), 201-225.

[16] Osher, S., & Sethian, J. A. (1988). Fronts propagating with curvature-dependent speed: Algorithms based on Hamilton-Jacobi formulations. *Journal of computational physics*, *79*(1), 12-49.

[17] Jacqmin, D. (1999). Calculation of two-phase Navier–Stokes flows using phase-field modeling. *Journal of computational physics*, *155*(1), 96-127.

[18] Kim, S., Ishii, M., Kong, R., & Wang, G. (2021). Progress in two-phase flow modeling: Interfacial area transport. *Nuclear Engineering and Design*, *373*, 111019.

[19] Yan, G., Li, Z., Galindo Torres, S. A., Scheuermann, A., & Li, L. (2022). Transient two-phase flow in porous media: a literature review and engineering application in geotechnics. *Geotechnics*, *2*(1), 32-90.

[20] Ala, A. A., Tan, S., Qiao, S., & Shiru, G. A. (2023). Simulation of the effect of partial and total blockage of a sub-channel on two-phase flow through a 5 x 5 square rod bundle. *Progress in Nuclear Energy*, *155*, 104514.

[21] Jalili, D., Jang, S., Jadidi, M., Giustini, G., Keshmiri, A., & Mahmoudi, Y. (2024). Physics-informed neural networks for heat transfer prediction in two-phase flows. *International Journal of Heat and Mass Transfer*, *221*, 125089.

[22] Fu, G., Wang, X., Wang, B., Su, J., Wang, K., & Sun, B. (2024). Dynamic behavior of axially functionally graded pipe conveying gas–liquid two-phase flow. *Applied Ocean Research*, *142*, 103827.

[23] Log, A. M., Hammer, M., Deng, H., Austegard, A., Hafner, A., & Munkejord, S. T. (2024). Depressurization of CO2 in a pipe: Effect of initial state on non-equilibrium two-phase flow. *International Journal of Multiphase Flow*, *170*, 104624.

[24] Xu, Y., Yang, G., & Hu, D. (2024). Comparison of surface tension models for the simulation of two-phase flow in an ISPH-FVM coupling method. *European Journal of Mechanics-B/Fluids*, *105*, 57-96.

[25] Iliyasu, A. M., Fouladinia, F., Salama, A. S., Roshani, G. H., & Hirota, K. (2023). Intelligent measurement of void fractions in homogeneous regime of two phase flows independent of the liquid phase density changes. *Fractal and Fractional*, *7*(2), 179.

[26] Amini, Y., Ghazanfari, V., Heydari, M., Shadman, M. M., Khamseh, A. G., Khani, M. H., & Hassanvand, A. (2023). Computational fluid dynamics simulation of two-phase flow patterns in a serpentine microfluidic device. *Scientific Reports*, *13*(1), 9483.

[27] Amini, Y., Ghazanfari, V., Heydari, M., Shadman, M. M., Khamseh, A. G., Khani, M. H., & Hassanvand, A. (2023). Computational fluid dynamics simulation of two-phase flow patterns in a serpentine microfluidic device. *Scientific Reports*, *13*(1), 9483.

[28] Ebrahimi-Mamaghani, A., Mostoufi, N., Sotudeh-Gharebagh, R., & Zarghami, R. (2022). Vibrational analysis of pipes based on the drift-flux two-phase flow model. *Ocean Engineering*, *249*, 110917.

[29] Shen, C., & Sun, M. (2022). Exact Riemann solutions for the drift-flux equations of two-phase flow under gravity. *Journal of Differential Equations*, *314*, 1-55.
[30] Jain, S. S. (2022). Accurate conservative phase-field method for simulation of two-phase flows. *Journal of Computational Physics*, *469*, 111529.
[31] Morse, R. W., Chan, J., Hurlburt, E. T., Le Corre, J. M., Berson, A., Nellis, G. F., & Dressler, K. M. (2024). A new paradigm for the role of disturbance waves on film dryout and wall heat transfer in annular two-phase flow. *International Journal of Heat and Mass Transfer*, *219*, 124812.
[32] Lin, Z., Sun, X., Yu, T., Zhang, Y., Li, Y., & Zhu, Z. (2020). Gas–solid two-phase flow and erosion calculation of gate valve based on the CFD-DEM model. *Powder Technology*, *366*, 395-407.